Journal of Power Sources 244 (2013) 29–34

Contents lists available at SciVerse ScienceDirect

Journal of Power Sources

journal homepage: www.elsevier.com/locate/jpowsour

Sodium additive to improve rate performance of $Li[Li_{0.2}Mn_{0.54}Ni_{0.13}Co_{0.13}]O_2$ material for Li-ion batteries

Ke Du [a,b,*], Fei Yang [a], Guo-rong Hu [a], Zhong-dong Peng [a], Yan-bing Cao [a], Kwang Sun Ryu [b]

[a] School of Metallurgical Science and Engineering, Central South University, Changsha, PR China
[b] Energy Harvest-Storage Research Center, University of Ulsan, Republic of Korea

HIGHLIGHTS

- Sodium additive induced a dispersed secondary phase with structure of $Na_{0.7}MnO_{2.05}$.
- The two-phase composite showed improved rate performance.
- Sodium additive enhanced electrical conductivity and lithium ionic conductivity.
- The sodium in the $Na_{0.7}MO_{2.05}$ can be activated for the transportation of Li^+.

ARTICLE INFO

Article history:
Received 12 October 2012
Received in revised form
31 December 2012
Accepted 30 April 2013
Available online 13 May 2013

Keywords:
Lithium-rich layered oxide
Sodium additive
Secondary phase
Rate performance

ABSTRACT

The effects of sodium additive on the microstructure and electrochemical properties of $Li[Li_{0.2}Mn_{0.54}Ni_{0.13}Co_{0.13}]O_2$-based material have been investigated. XRD patterns show that the sodium additive doesn't incorporate into the $Li[Li_{0.2}Mn_{0.54}Ni_{0.13}Co_{0.13}]O_2$ lattice, but induces a dispersed secondary phase with the structure of $Na_{0.7}MnO_{2.05}$. The two-phase composite shows an improved rate performance in comparison with the single phase of $Li[Li_{0.2}Mn_{0.54}Ni_{0.13}Co_{0.13}]O_2$, which can be attributed to the enhanced electrical conductivity and lithium ion diffusion. The interfaces between $Li[Li_{0.2}Mn_{0.54}Ni_{0.13}Co_{0.13}]O_2$ and the secondary phase provide fast diffusion paths for Li^+. DC electrical conductivity and EIS are used to elucidate the phenomenon.

1. Introduction

Lithium-rich layered oxides, within the system of $xLi[Li_{1/3}Mn_{2/3}]O_2\cdot(1-x)LiMO_2$ where M is one or more transition metal ion, are becoming attractive for their extraordinarily high capacity, low cost and safety [1]. They demonstrate a very high capacity of about 250 mAh g^{-1} when charged to 4.6 V or higher [2–4]. The capacity of $xLi_2MnO_3\cdot(1-x)LiNi_{1/3}Co_{1/3}Mn_{1/3}O_2$ reaches up to 300 mAh g^{-1} at high temperature (50 °C) and low current density (0.05 mA cm^{-2}) [5]. However, the disadvantage of poor rate capability restricts the practical application of the high capacity material [1].

Cathode materials of lithium batteries are mixing conductor of electron and lithium ion, which absorb and release energy by the simultaneous extraction and insertion of electrons and Li^+ ions. Hence, the rate capability of cathode materials will depend critically on the rate at which the electrons and Li^+ ions can migrate through the electrolyte and composite electrode structure into the active electrode material. Strategies to increase the low rate performance of cathode materials have focused on improving electron transport in the bulk [6] or at the surface of the material [7,8], or on reducing the path length over which the electron and Li^+ ion have to move by using nano-sized materials [9,10].

For lithium-rich layered oxides, a thick solid–electrolyte interfacial layer (SEI) will form between the cathode surface and the electrolyte when they are continuously charged to 4.8 V [11], which causes the poor surface conductivity. To solve this problem, the first possible attempt is to reduce particle size or synthesis well crystallized nanometer materials [12]. However, it will increase the specific surface area and decrease the density. The second method is to coat the cathode surface with conductive agents such as Al [13] or carbon [14], which forms composite materials with improved rate performance due to the better surface electrical conductivity. The third strategy is surface modification, which is to

* Corresponding author. School of Metallurgical Science and Engineering, Central South University, Changsha, PR China. Tel.: +86 731 88876454.
E-mail addresses: duke22@csu.edu.cn, dukeben1976@yahoo.com (K. Du).

0378-7753/$ – see front matter © 2013 Elsevier B.V. All rights reserved.
http://dx.doi.org/10.1016/j.jpowsour.2013.04.152

change the surface of the material to a spinel structure, such as $LiMn_2O_4$, $LiNi_{0.5}Mn_{1.5}O_4$ or $Li_4Mn_5O_{12}$ [15,16]. The spinel on the surface can provide three-dimensional (3D) diffusion paths to help Li transfer through the surface of cathodes at high current densities.

Sodium ion has a larger radius than that of lithium ion (108 pm vs. 76 pm), so sodium was used as a pillaring species between MnO_2 layers in $Na_{0.45}MnO_{2.14}\cdot0.76H_2O$ [17]. Kim et al. reported a series of layered $Na_xLi_yNi_{0.25}Mn_{0.75}O_\delta$ oxides within the range of $0.7 \le x \le 1.2$ and $0 < y \le 0.5$ that could be easily synthesized by a solid state method and showed good rate capability in sodium ion batteries [18]. At the same time, some sodium containing materials such as $Na_3V_2(PO_4)_2F_3$ and $NaV(PO_4)F$ were used successfully as cathodes in lithium ion batteries with satisfied rate performance [19,20].

Bearing these in mind, we tried to introduce sodium into lithium-rich layered oxides. If sodium substitutes lithium partly in lithium-rich layered oxides as a pillaring species, the space between layers of the oxides will be increased and the transferring channel for lithium ion will be enlarged. Improved rate performance can be expected. However, it was found in our experiments that the formation of a two-phase system rather than the substitution of Li by Na occurred when sodium was used to replace lithium in lithium-rich layered oxides.

In this work, we reported a series of compounds with nominal formula of $Na_xLi_{1.2-x}Mn_{0.54}Ni_{0.13}Co_{0.13}O_2$ $(0 \le x \le 0.3)$ synthesized via a co-precipitation method and followed by a solid-state reaction at high temperature. The structural, morphology and electrochemical performance of prepared materials were investigated.

2. Experimental

The precursor of $Mn_{0.54}Ni_{0.13}Co_{0.13}(CO_3)_{0.8}$ was synthesized by a co-precipitation method. Stoichiometric amounts of $MnSO_4\cdot H_2O$ (Xilong Group, 99%), $NiSO_4\cdot 6H_2O$ (Sinopharm Chemical Reagent, 98%) and $CoSO_4\cdot 7H_2O$ (Sinopharm Chemical Reagent, 99%) were dissolved in deionized water to prepare a 1 M mixed metal ion aqueous solution. A 1 M aqueous solution of sodium carbonate was used as the precipitator and a 0.8 M aqueous solution of ammonium bicarbonate was used as the chelating agent. The above three solutions were pumped into a continuously stirred 10 L tank reactor (Xiaoxuan, China). The temperature and pH value of the solution were controlled at 50 °C and 8.5, respectively. The obtained mixed metal ion carbonate precipitate was then filtered, washed and dried at 60 °C in air for 24 h. The carbonate precursor was then heated at 500 °C for 6 h to form an oxide precursor $Mn_{0.54}Ni_{0.13}Co_{0.13}O_{1.6}$. After component analysis, the oxide precursor was mixed with Li_2CO_3, Na_2CO_3 with nominal cation composition of Li:Na:(Mn + Ni + Co) = $(1 - x):x:0.8$. The mixture was then annealed at 900 °C for 10 h to obtain the final products with nominal formula $Na_xLi_{1.2-x}Mn_{0.54}Ni_{0.13}Co_{0.13}O_2$ (x = 0, 0.05, 0.1, 0.2 and 0.3, hereafter those samples are represented by N0, N05, N1, N2 and N3 in sequence).

Powder X-ray diffraction (XRD, Rigaku, Rint-2000) using Cu Kα radiation was employed to identify the crystalline phase of the prepared powders. XRD data were obtained at $2\theta = 10$–$80°$, with a scan speed of $0.01° s^{-1}$. The microstructure of material was collected with scanning electron microscopy (SEM, JSM-6360LV).

The elemental contents of lithium and sodium in the cathode materials were determined by inductively coupled plasma atomic emission spectroscopy (ICP-AES).

The materials were pressed into pellets of 12 mm diam and about 0.55 mm thickness. Their conductivities were measured by Van der Pauw four-point direct current (dc) method on a four point probing system (HMS-3000/0.55T).

The Brunauer, Emmett, and Teller (BET) surface area was analyzed by using Beckman Coulter SA3100.

Charge–discharge tests were performed using coin type cells (CR2025). The cell consisted of the positive and the lithium metal negative electrodes separated by a porous polypropylene film. The positive electrode was prepared by blending active material, carbon black and polyvinylidene fluoride (80:10:10) in *N*-methyl-2-pyrrolidone. The slurry was then cast on an aluminum foil and dried at 120 °C overnight under vacuum. The electrolyte solution was 1 M $LiPF_6$ in a mixture of ethylene carbonate (EC) and diethyl carbonate (DEC) at a 1:1 volume ratio. Cells were cycled galvanostatically on Land battery testing system at room temperature.

Electrochemical impedance spectroscopy (EIS) analysis was carried out from 100 kHz to 10 mHz by using the potentiostat/galvanostat Model 2273A potentiostat and the Model 5210 lock-in amplifier with 5 mV ac distribution.

3. Results and discussion

3.1. Crystal structure and morphology

Fig. 1 shows X-ray diffraction patterns of N0, N05, N1, N2 and N3. All Bragg diffraction lines of N0 are assigned to a rhombohedral lattice with a space group *R-3m* (no. 166) except broad peaks found in the two theta range of 20–25 degrees. The broad peaks can be assigned to superlattice ordering peaks, which originate from Li and transition metal elements ordering in transition metal layers (3a sites). However, for N2 and N3, there are several extra peaks, which can be well assigned to a new phase with the structure of $Na_{0.7}MnO_{2.05}$ (JCPDS 27-0751). Here it is $Na_{0.7}(Mn_{0.675}Ni_{0.1625}Co_{0.1625})O_{2.05}$ (represented by $Na_{0.7}MO_{2.05}$ in following text). And with the increase of sodium, the peaks corresponding to the new phase become stronger meaning the increase of the amount of $Na_{0.7}MO_{2.05}$.

The lattice parameters of samples are calculated by fitting all *R-3m* peaks and listed in Table 1. For the pure $Li[Li_{0.2}Mn_{0.54}Ni_{0.13}Co_{0.13}]O_2$ (N0), the parameters are $a = 2.8543$ Å and $c = 14.2489$ Å. They decrease obviously when some amount of sodium element is introduced into the composite ($x = 0.05$). At present stage, we can't explain why the crystalline parameters shrink suddenly with the small amount of Na additive. However, it seems that sodium ions don't substitute any lithium ions in the mother material because the ion radius of Na^+ (102 pm) is much larger than that of Li^+ (76pm). On the other hand, the parameter c shows an increased trend with the amount of Na additive increasing. This can be understood within the $Li_{1.2+\delta}[Mn_{0.54}Ni_{0.13}Co_{0.13}]O_2$–$Na_{0.7}MO_{2.05}$

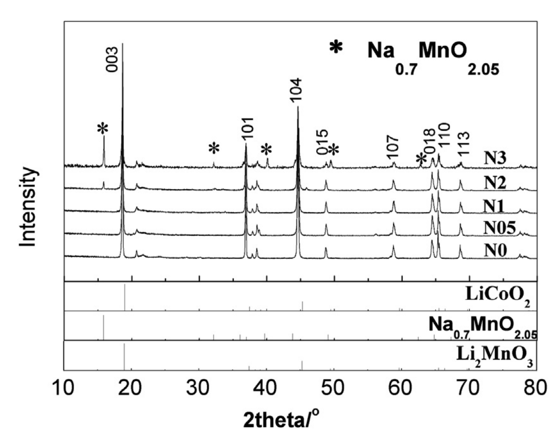

Fig. 1. XRD patterns of $Na_xLi_{1.2-x}Mn_{0.54}Ni_{0.13}Co_{0.13}O_2$ (x = 0, 0.05, 0.1, 0.2, 0.3).

Table 1
Lattice parameters of five samples with nominal formula $Na_xLi_{1.2-x}Mn_{0.54}Ni_{0.13}Co_{0.13}O_2$ ($x = 0, 0.05, 0.1, 0.2, 0.3$).

Sample	Lattice parameter/Å		
	a	*c*	*c/a*
N0($x = 0$)	2.8543	14.2489	4.992
N05($x = 0.05$)	2.8525	14.2344	4.990
N1($x = 0.1$)	2.8528	14.2369	4.990
N2($x = 0.2$)	2.8529	14.2409	4.992
N3($x = 0.3$)	2.8515	14.2475	4.997

two-phase system. It is the sample of N0 for $\delta = 0$, $Li[Li_{0.2}Mn_{0.54}Ni_{0.13}Co_{0.13}]O_2$. $Na_{0.7}MO_{2.05}$ new phase forms when Na additive is introduced into the system ($\delta > 0$), which has a lower ratio of basic metal over transition metal (0.7) than that of $Li[Li_{0.2}Mn_{0.54}Ni_{0.13}Co_{0.13}]O_2$ (1.5), in turn, causes extra lithium enter the transition metal layer of $Li[Li_{0.2}Mn_{0.54}Ni_{0.13}Co_{0.13}]O_2$ to form $Li_{1.2+\delta}[Mn_{0.54}Ni_{0.13}Co_{0.13}]O_2$ that increases the lattice parameter *c*. Lithium rich layered oxides with more than 1.2 mol Li^+ per formulus has been reported by some authors [21,22].

The clear peak split of (108, 110) pair and the high *c/a* ratio (>4.899) for all five samples are known to be an indicator of good layered structure.

The SEM images of the precursor powders $Mn_{0.54}Ni_{0.13}Co_{0.13}(CO_3)_{0.8}$, pure phase $Li[Li_{0.2}Mn_{0.54}Ni_{0.13}Co_{0.13}]O_2$ (N0) and four two-phase composites (N05, N1, N2 and N3) are shown in Fig. 2. The precursor synthesized by the co-precipitation method appears as uniform spherical particles with average diameter of several micrometers. But the final products lose the spherical morphology after ball-milling and calcination, which show homogeneous particle size at about 0.5 μm and no clear difference with different Na additive.

3.2. Charge–discharge characteristics

The initial charge and discharge profiles of N0, N05, N1, N2 and N3 at 0.1 C rate are plotted in Fig. 3. Pure phase $Li[Li_{0.2}Mn_{0.54}Ni_{0.13}Co_{0.13}]O_2$ delivers a high capacity of 241.9 mAh g^{-1}. With Na additive increasing, the discharge capacity at 0.1 C decreases to

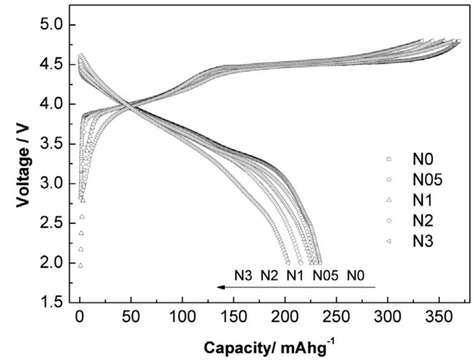

Fig. 3. Initial charge and discharge curves of $Na_xLi_{1.2-x}Mn_{0.54}Ni_{0.13}Co_{0.13}O_2$ ($x = 0, 0.05, 0.1, 0.2, 0.3$) at 0.1 C.

235 mAh g^{-1} for N05, 221.6 mAh g^{-1} for N1, 215.6 mAh g^{-1} for N2 and 209.0 mAh g^{-1} for N3, respectively. Such decrease of capacity at a low discharge rate is mainly caused by the increasing amount of the secondary phase of $Na_{0.7}MO_{2.05}$ as shown in the XRD. According to our another experiment (not shown here), $Na_{0.7}[Mn_{0.54}Ni_{0.13}Co_{0.13}]O_{2.05}$ is active for the transportation of Li^+ by exchange with lithium in the electrolyte as $Na_3V_2(PO_4)_2F_3$ and $NaV(PO_4)F$ do [19,20]. It can deliver about 150 mAh g^{-1} between 2 and 4.8 V, which is much lower than that of $Li[Li_{0.2}Mn_{0.54}Ni_{0.13}Co_{0.13}]O_2$.

The rate capability of N0, N05, N1, N2 and N3 is shown in Fig. 4. Cells are continuously charged and discharged at different C-rates. The charge rate for the first 5 cycles and the last 5 cycles is 0.1 C, but 0.2 C for the middle 35 cycles. The discharge rate changes from 0.1 to 0.2, 0.5, 1, 2, 3, 4, 5 and 0.1 C for every continued 5 cycles. The average values of discharge capacity in five cycles at each rate are listed in Table 2. The results indicate that the discharge capacity decreases rapidly with discharge rate increasing for all samples, but it is more slowly for Na additive samples. For example, the capacity at 1 C is 149.5 mAh g^{-1} for N0, but 159.6, 163.5, 174.5 and 169.3 mAh g^{-1} for N05, N1, N2 and N3, respectively. At 5 C, only 66.3 mAh g^{-1} can be delivered by N0, but 135.6 mAh g^{-1} by N2. It is obvious that the additive of sodium improves the rate capability. Because it is unlikely for sodium to take position of lithium in the

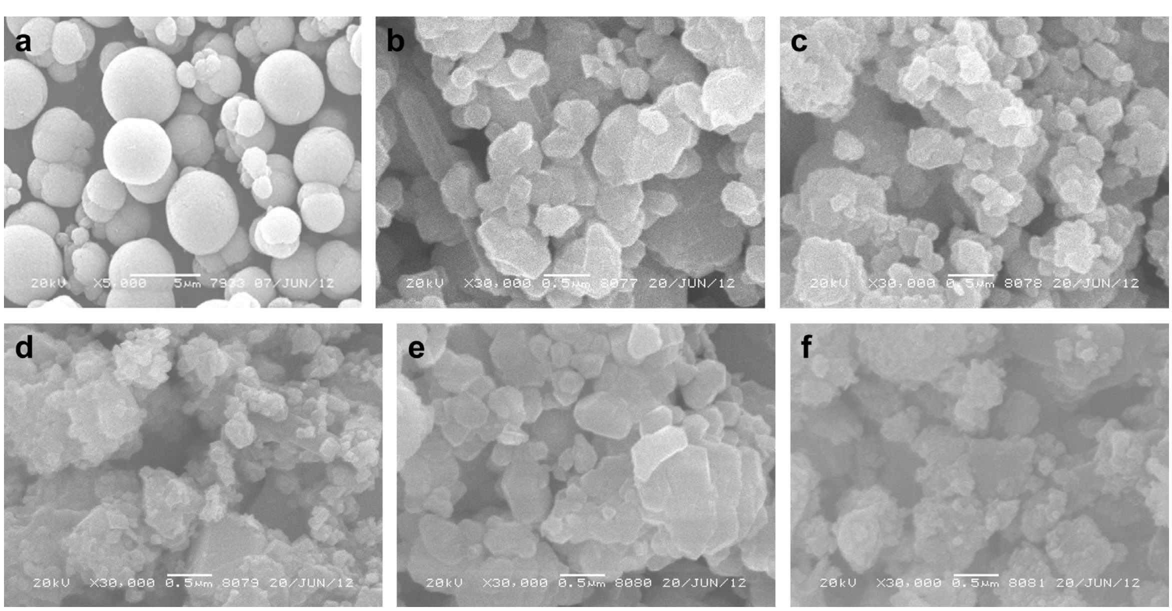

Fig. 2. SEM images of $Na_xLi_{1.2-x}Mn_{0.54}Ni_{0.13}Co_{0.13}O_2$ (a: carbonate co-precipitation; b: N0; c: N05, d: N1, e: N2, f: N3).

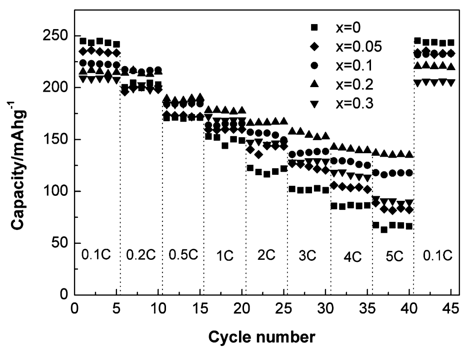

Fig. 4. Discharge capacities of $Na_xLi_{1.2-x}Mn_{0.54}Ni_{0.13}Co_{0.13}O_2$ ($x = 0, 0.05, 0.1, 0.2, 0.3$) at different C-rates.

layer structure of $Li[Li_{0.2}Mn_{0.54}Ni_{0.13}Co_{0.13}]O_2$, as shown by lattice parameters, the source of ameliorative rate performance is attributed to the existence of the secondary phase $Na_{0.7}MO_{2.05}$. However, the improvement isn't in a direct proportion to the amount of the secondary phase and $x = 0.2$ is the optimized value in our experiment.

In order to understand the effect of the secondary phase of $Na_{0.7}MO_{2.05}$ on the charge–discharge process, we investigated the change of element concentration of lithium and sodium in N2 composite. The measurements are made before cycle, after one and sixty cycles. The cells experienced cycles are disassembled in the Ar-filled glove box. The positive electrodes are soaked and rinsed with dimethyl carbonates DMC for three times. After dried in the glove box at room temperature, the remaining cathode materials are blown down and dissolved in hydrochloric acid, then filtered in order to remove the insoluble carbon black. The ICP analysis results are shown in Table 3.

It can be found that lithium content decreases from 8.86% to 6.38% after the first cycle, which is due to the irreversible initial capacity loss and the formation of SEI film in the first cycle. It is interested that lithium content rises to 7.04% after 60 cycles. On the other hand, sodium content dives from initial value of 5.11% to 2.00% in the first cycle, and decreases slowly to 1.92% at the end of the 60th cycle. The phenomenon indicates that the sodium in the secondary phase $Na_{0.7}MO_{2.05}$ can be activated for the transportation of Li^+ by exchanging with lithium in the electrolyte. The reaction mechanism is similar to that of $Na_3V_2(PO_4)_2F_3$ or $NaV(PO_4)F$ in lithium ion battery system [19,20]. In our materials, the exchange process between sodium and lithium happens mainly during the first cycle and some amount of sodium can't be exchanged even after many cycles.

3.3. Electrical conductivity and EIS

In order to explain the reason of improved rate performance by Na additive, we compared the migration of electron and lithium ion

Table 2
Discharge capacities at different C-rates of five samples with nominal formula $Na_xLi_{1.2-x}Mn_{0.54}Ni_{0.13}Co_{0.13}O_2$ ($x = 0, 0.05, 0.1, 0.2, 0.3$).

Samples	Discharge specific capacity/mAh g^{-1}							
	0.1 C	0.2 C	0.5 C	1 C	2 C	3 C	4 C	5 C
N0($x = 0$)	243.6	202.5	171.0	149.6	119.7	101.7	86.1	66.3
N05($x = 0.05$)	234.7	198.8	172.9	159.7	141.4	123.9	104.0	83.9
N1($x = 0.1$)	222.8	216.5	184.3	164.5	154.6	137.3	127.7	117.4
N2($x = 0.2$)	215.2	214.5	188.9	177.8	166.4	154.8	140.9	135.6
N3($x = 0.3$)	208.7	199.6	184.7	169.4	146.8	128.8	116.2	90.5

Table 3
Weight percent of elements lithium and sodium in N2 composite.

Element	Content		
	Before cycle	After 1st cycle	After 60th cycle
Li	8.86%	6.38%	7.04%
Na	5.11%	2.00%	1.92%

of the five samples by testing their DC conductivity and electrochemical impedance spectroscopy.

The electrical conductivities of the samples have been measured as a function of Na content at room temperature (Fig. 5). The electrical conductivity value is 3.9×10^{-3} S cm^{-1} for pure Li $[Li_{0.2}Mn_{0.54}Ni_{0.13}Co_{0.13}]O_2$ (N0). For Na additive samples, electrical conductivities are improved by 3–6 times. For example, it is 1.9×10^{-2} S cm^{-1} for N2.

The effect of the Na introduction was also investigated by EIS measurement. N0 and N2 were chosen for analysis. The cells, $Li[Li_{0.2}Mn_{0.54}Ni_{0.13}Co_{0.13}]O_2/Li$ and $Na_{0.2}LiMn_{0.54}Ni_{0.13}Co_{0.13}O_2/Li$, were first charged and discharged at 0.1 C for five times. The EIS of the cells at five states of charge (SOC): 20, 40, 60, 80 and 100% and two states of discharge (SOD): 66 and 33% were studied. The cells rested for 5 h before the EIS measurements.

The Nyquist plots of the 60% SOC and 66% SOD are plotted in Fig. 6a and b (the plots of other states are similar). These plots consist of two semicircle at high and medium frequency regions followed a line in the low frequency region. They were analyzed by Zview software and fitted very well by an equivalent circuit shown in Fig. 6c. According to Refs. [23–25], R_b represents the solution resistance, the semicircle at high frequency represents resistance of the solid-state interface layer (R_{sei}), the semicircle at the medium frequency represents resistance of charge transfer (R_{ct}) and the sloping line at low frequency is ascribed to the basic metal ions diffusion in the layered oxide material. The calculated R_{sei} and R_{ct} are listed in Table 4 and it can be found that the sodium additive sample N2 exhibits much lower charge-transfer impedances than N0 at each SOC or SOD. These results show that Na additive improves the general electrochemical impedance characteristics.

The ion diffusion coefficient can be calculated by Eq. (1)

$$D = \frac{0.5R^2T^2}{S^2n^4F^4C^2\sigma^2} \tag{1}$$

R and F are the gas and Faraday constant, respectively. T is the absolute temperature, S is the active surface area of the electrode, in our work it is 4.369 m^2 g^{-1} for N0 and 4.703 m^2 g^{-1} for N2

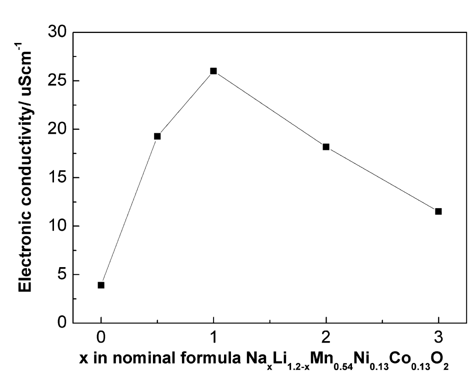

Fig. 5. DC conductivity of $Na_xLi_{1.2-x}Mn_{0.54}Ni_{0.13}Co_{0.13}O_2$ ($x = 0, 0.05, 0.1, 0.2, 0.3$).

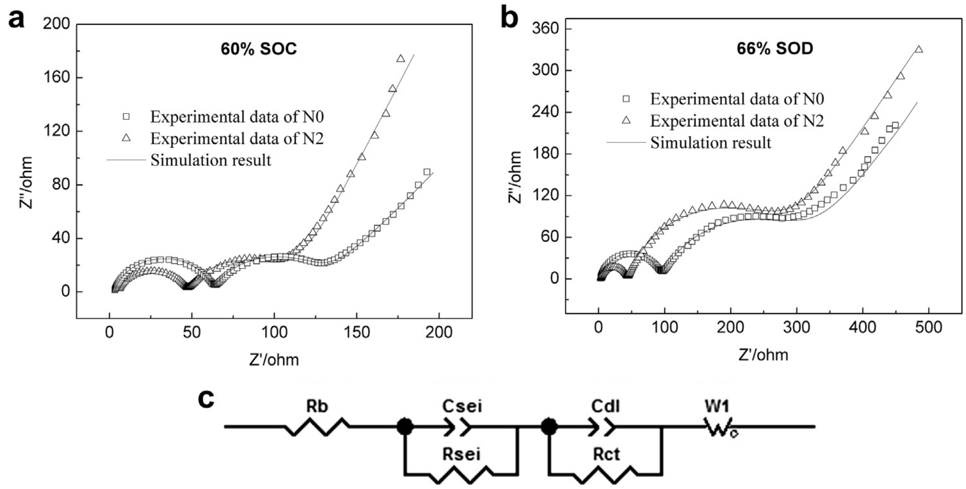

Fig. 6. (a) The experimental data and simulation result of Nyquist plots at 60% SOC (N0 and N2). (b) The experimental data and simulation result of Nyquist plots at 66% SOD (N0 and N2). (c) The equivalent circuits to fit the Nyquist plots of the electrochemical impedance spectra.

respectively. n is the number of electrons transfer per unit, C is the concentration of basic metal ions (Li^+ and Na^+) in the active material, which can be obtained by calculating the concentration of crystallography and the state of charge or discharge. σ is Warburg factor that is determined by Eq. (2)

$$Z' = R1 + R2 + R3 + \sigma\omega^{-1/2} \tag{2}$$

Z' is the image impedance and ω is the frequency. σ can be gotten by linear fitting $Z'{-}\omega^{-1/2}$ plot. Then the ion diffusion coefficient can be calculated by Eq. (1). The results of σ and D are listed in Table 4. It is noted that here the ion diffusion coefficient is the mixed value of Li^+ and Na^+. Both N0 and N2 show ion diffusion coefficient of about 10^{-14} cm^2 S^{-1} during the charge process and $10^{-16}\sim10^{-15}$ cm^2 S^{-1} during the discharge process. The full charged state shows the smallest value with the magnitude of 10^{-17} cm^2 S^{-1}. However, the ion diffusion coefficient of N2 is larger than that of N0 at every state. So the secondary phase of $Na_{0.7}MO_2$ enhances the basic metal ions diffusion in lithium-rich layered oxides.

Fig. 7 demonstrates the Nyquist plots of the cells constructed with N0, N05, N1, N2 and N3 after 50 cycles. The charge-transfer impedances calculated from the Nyquist plots were 426, 310, 198, 122, 174 Ω for N0, N05, N1, N2, N3 respectively. The sodium additive samples exhibit much lower charge-transfer impedances while N2 shows the smallest one.

It is commonly considered that the rate behavior of charge–discharge is closely connected with the charge transfer occurring at the cathode/electrolyte interface and the Li^+ diffusion in the active material. The rate of $Li[Li_{0.2}Mn_{0.54}Ni_{0.13}Co_{0.13}]O_2$ is commonly believed to be limited at the surface [11]. In our Na additive two-phase system, the structure in interfaces between phases is loose and the phase interfaces can provide fast diffusion paths for atomic and ionic transportation. The introduction of a dispersive secondary phase particles into an ionic conductor can result in an increase in the ionic conductivity [26]. Here, in the Na additive two-phase composite, the stabilization of grain boundaries was accomplished by introducing a secondary phase. The interfaces among $Li[Li_{0.2}Mn_{0.54}Ni_{0.13}Co_{0.13}]O_2$ and $Na_{0.7}MO_{2.05}$ provide the fast diffusion paths of Li^+, i.e. the diffusion of Li^+ in the oxide particle is also enhanced by the interface diffusion. As a result, the discharge capacity at high rates may be improved. The superior high rate performance of two-phase materials as active materials of electrode was also reported in $LiCoO_2$–TiO_2 system for lithium ion battery [27].

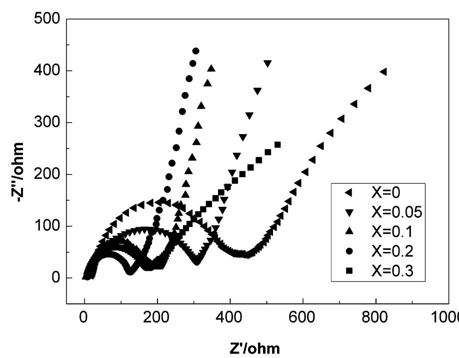

Fig. 7. Impedance spectra of $Na_xLi_{1.2-x}Mn_{0.54}Ni_{0.13}Co_{0.13}O_2$ ($x = 0$, 0.05, 0.1, 0.2, 0.3).

Table 4
The impedance parameters of N0 and N2.

State	N0				N2			
	R_{sei}/Ω	R_{ct}/Ω	σ	D/cm^2 S^{-1}	R_{sei}/Ω	R_{ct}/Ω	σ	D/cm^2 S^{-1}
20% SOC	86.1	144.9	6.980	1.502×10^{-14}	72.0	82.1	5.912	1.807×10^{-14}
40% SOC	59.9	82.2	6.612	1.560×10^{-14}	41.6	38.3	5.630	1.993×10^{-14}
60% SOC	59.4	63.5	4.753	3.239×10^{-14}	40.0	32.4	4.2107	3.562×10^{-14}
80% SOC	50.7	117.4	3.251	6.923×10^{-14}	33.0	107.8	2.989	7.070×10^{-14}
100% SOC	50.0	2986	118.14	5.243×10^{-17}	29.6	1231	98.915	6.455×10^{-17}
33% SOD	64.2	251.7	35.19	5.912×10^{-16}	36.1	163.3	24.577	7.432×10^{-16}
66% SOD	90.35	212.7	13.40	4.079×10^{-15}	79.6	211.6	11.148	5.082×10^{-15}

4. Conclusion

Different amount of Na additive was introduced into Li$[Li_{0.2}Mn_{0.54}Ni_{0.13}Co_{0.13}]O_2$ by simple solid state reaction. Sodium ions don't take the position of lithium ions but form a secondary phase with the structure of $Na_{0.7}MnO_{2.05}$. The rate performance of the layer oxides is improved in the Na additive two-phase system, for example, sample N2 with nominal composition $Na_{0.2}LiMn_{0.54}Ni_{0.13}Co_{0.13}O_2$ can deliver 174.5 mAh g^{-1} at 1 C and 135.6 mAh g^{-1} at 5 C. The improved rate performance of Na additive two-phase system is ascribed to enhanced electrical conductivity and ion diffusion.

References

[1] M.M. Thackeray, S.-H. Kang, C.S. Johnson, J.T. Vaughey, R. Benedek, S.A. Hackney, J. Mater. Chem. 17 (2007) 3112–3125.
[2] Z. Lu, D.D. MacNeil, J.R. Dahn, Electrochem. Solid State Lett. 4 (2001) A191–A194.
[3] A.R. Armstrong, A.D. Robertson, P.G. Bruce, J. Power Sources 146 (2005) 275–280.
[4] X.J. Guo, Y.X. Li, M. Zheng, J.M. Zheng, J. Li, Z.L. Gong, Y. Yang, J. Power Sources 184 (2008) 414–419.
[5] C.S. Johnson, N. Li, C. Lefief, M.M. Thackeray, Electrochem. Commun. 9 (2007) 787–795.
[6] S.Y. Chung, J.T. Bloking, Y.M. Chiang, Nature Mater. 1 (2002) 123–128.
[7] N.C.Y. Ravet, J.F. Magnan, S. Besner, M. Gauthier, M. Armand, J. Power Sources 97 (2001) 503–507.
[8] P.S. Herle, B. Ellis, N. Coombs, L.F. Nazar, Nature Mater. 3 (2004) 147–152.
[9] C. Delacourt, P. Poizot, S. Levasseur, C. Masquelier, Electrochem. Solid State Lett. 9 (2006) A352–A355.
[10] D.H. Kim, J. Kim, Electrochem. Solid State Lett. 9 (2006) A439–A442.
[11] Q.Y. Wang, J. Liu, A.V. Murugan, A. Manthiram, J. Mater. Chem. 19 (2009) 4965–4972.
[12] W. He, J. Qian, Y. Cao, X. Ai, H. Yang, RSC Adv. 2 (2012) 3423–3429.
[13] A.R. Armstrong, M. Holzapfel, P. Novak, J. Am. Chem. Soc. 128 (2006) 8694–8698.
[14] M.A. Hashem, A.E. Abdel-Ghany, A.E. Eid, J. Trottier, K. Zaghib, A. Mauger, C.M. Julien, J. Power Sources 196 (2011) 8632–8637.
[15] D.Y.W. Yu, K. Yanagida, H. Nakamura, J. Electrochem. Soc. 157 (2010) A1177–A1182.
[16] M.M. Thackeray, C. S. Johnson, N.C. Li, US Patent No. 7303840 B2 (4 Dec, 2007).
[17] P.L. Goff, N. Baffier, S. Bach, J.P. Pereira-Ramos, R. Messina, Solid State Ionics 61 (1993) 309–315.
[18] D. Kim, S.-H. Kang, M. Slater, S. Rood, J.T. Vaughey, N. Karan, M. Balasubramanian, C.S. Johnson, Adv. Energy Mater. 1 (2011) 333–336.
[19] J. Barker, R.K.B. Gover, P. Burns, A.J. Bryan, Electrochem. Solid State Lett. 9 (2006) A190–A192.
[20] J. Barker, M.Y. Saidi, J.L. Swoyer, J. Electrochem. Soc. 151 (2004) A1670–A1677.
[21] H. Deng, I. Belharouak, H. Wu, D. Dambournet, K. Amine, J. Electrochem. Soc. 157 (2010) A776–A781.
[22] H. Deng, I. Belharouak, R.E. Cook, H. Wu, Y.K. Sun, K. Amine, J. Electrochem. Soc. 157 (2010) A447–A452.
[23] J. Liu, B.R. Jayan, A. Manthiram, J. Phys. Chem. C 114 (2010) 9528–9533.
[24] A.-K. Hjelm, G. Lindbergh, Electrochim. Acta 47 (2002) 1747–1759.
[25] S.S. Zhang, K. Xu, T.R. Jow, Electrochim. Acta 49 (2004) 1057–1061.
[26] C.C. Liang, J. Electrochem. Soc. 120 (1973) 1289–1292.
[27] Choblet, H.C. Shiao, H.-P. Lin, M. Salomon, V. Manivannan, Electrochem. Solid State Lett. 4 (2001) A65–A67.